Modelling and analysis of glucocorticoid action in acute lymphoblastic leukemia

AISHA OTHMAN[1], HEND ALRASHEEDI[2,3], MUHAMMAD-NURUDEEN NURUDEEN[1], DELTA PATRICIA MENENDEZ CREAMER[1], ALIREZA FATAHIAN[1], CONSTANTINOS DEMONACOS[2], ATHAR AZIZ[1], MARIJA KRSTIC-DEMONACOS[1*] and EMYR YOSEF BAKKER[4*]

[1]School of Science, Engineering and Environment, University of Salford, Salford, Manchester M5 4WT, UK; [2]School of Health Sciences, University of Manchester, Manchester M13 9PL, UK; [3]King Saud University, Riyadh 11461, Kingdom of Saudi Arabia; [4]School of Medicine and Dentistry, University of Lancashire, Preston PR1 2HE, UK

Received February 3, 2026; Accepted September 18, 2026

DOI: 10.3892/ijo.2026.5963

Abstract. Glucocorticoids (GCs) induce apoptosis in leukocytes and remain a cornerstone of acute lymphoblastic leukemia (ALL) therapy, though resistance and toxicity remain problems. GEB052, a previously published Boolean model of the glucocorticoid receptor (GR) and its connected proteins, input (GC) and outputs (cell death and inflammation), generated insight into glucocorticoid resistance. The present study improved the model's predictive capacity through the inclusion of 26 microRNAs (miRs), resulting in a new model: GAO078 (78 nodes, 274 edges). GAO078 demonstrated improved correct prediction rates compared with GEB052, while dependency matrix and DRUGSURV analyses, together with laboratory validation, identified signal transducer and activator of transcription 5B (STAT5B) as an important level of control linked to GCs and apoptosis. The tyrosine kinase inhibitor dasatinib (DAS), which targets STAT5B and conventionally targets break point cluster (BCR)-Abelson tyrosine kinase gene (ABL), was shown in ALL cell lines to have selective efficacy for GC-resistant cells. Notably, cytotoxicity was demonstrated for BCR-ABL-negative leukemic cells, suggesting the potential for the use of DAS in this type of leukemia cells, upon further testing. GAO078 model analysis also identified miR-27a, miR-20a and miR-9 to feature frequently and have clinical significance. Laboratory analysis of dexamethasone/DAS-treated ALL cells showed an increase in the expression of these miRs. All three miRs are predicted to target nuclear receptor coactivators and corepressors; therefore, the outcome on nuclear receptor action could be a balance between multiple, complex networks. The findings of the present study demonstrate the significance of GR signaling and microRNA crosstalk in the determination of cell fate and emphasize the value of a systems biology approach in helping to identify routes towards reducing GC resistance and potentially improving future leukemia treatment.

Correspondence to: Professor Marija Krstic-Demonacos, School of Science, Engineering and Environment, University of Salford, Cockcroft Building, The Crescent, Salford M5 4WT, UK
E-mail: m.krstic-demonacos@salford.ac.uk

Dr Emyr Yosef Bakker, School of Medicine and Dentistry, University of Lancashire, Harrington Building, 11 Victoria St, Preston PR1 2HE, UK
E-mail: ebakker@lancashire.ac.uk

*Contributed equally

Abbreviations: ABL, Abelson tyrosine kinase gene; ALL, acute lymphoblastic leukemia; B-ALL, B-cell acute lymphoblastic leukemia; BCR, break point cluster; DAS, dasatinib; DM, dependency matrix; DEX, dexamethasone; DCC, dextran coated charcoal; GR, glucocorticoid receptor; GCs, glucocorticoids; LSSA, logical steady state analysis; miRs, microRNAs; STAT5B, signal transducer and activator of transcription 5B; STSFA, signal transduction score flow algorithm

Key words: acute lymphoblastic leukemia, bioinformatics, glucocorticoid receptor, miRNAs

Introduction

Acute lymphoblastic leukemia (ALL) is a malignant bone marrow disorder in which precursor lymphoblasts are altered, leading to dysregulated and increased proliferation (1). Treatment of ALL includes, but is not limited to, glucocorticoids (GCs), vincristine, daunorubicin and asparaginase. GCs are an important part of chemotherapeutic regimens for the treatment of leukemia due to their ability to cause apoptosis in white blood cells. This is mainly through affecting BCL2 family members, though links to autophagy and necroptosis have also been posited (2,3). GCs commonly used in the clinic include prednisone, prednisolone and dexamethasone and they have been instrumental in improving the survival of ALL patients (4). Synthetic GCs are commonly used in the therapy of hematological malignancies due to their greater potency and stability. However, steroid resistance and associated toxicities need to be researched and understood to improve patient outcomes further.

GCs are steroid hormones which play a vital role in homeostasis, the stress response, carbohydrate metabolism and water and electrolyte balance, as well as regulating

the immune response (5). GCs function mostly through interacting with the glucocorticoid receptor (GR), a ligand-regulated transcription factor which is a member of the superfamily of nuclear hormone receptors. In the absence of a ligand, GR exists in the cytoplasm as part of a multiprotein complex including heat-shock proteins. Following ligand binding, these heat-shock proteins dissociate, which exposes the nuclear localization signal, thus facilitating nuclear translocation. GR is present in most cell types, and upon ligand binding and nuclear translocation, it is recruited to GC response elements, activating or suppressing the expression of its transcription target genes in a cell-type-specific manner (6).

GR action is affected, at least in part, by microRNAs (miRs) (7) which are non-coding genetic elements that inhibit translation (1) and affect gene regulation (8). MiRs are known to participate in leukemia pathogenesis and have potential as biomarkers for diagnosis and relapse monitoring (8).

The importance of GCs in leukemia prompted previous modelling work which captured the GR and its signaling partners (the GEB052 model, 'GR interactome') through a systems biology approach (9). GEB052 consisted of the GR, 48 linked genes/proteins, as well as an input (GC) and outputs of cell death and inflammation (9). This model demonstrated good predictive utility, led to novel molecular insights and was preliminarily validated as a clinical tool. However, it did not incorporate wider genetic elements such as miRs. Thus, the present study built on the GEB052 model by including miRs and validated the new model's predictions in the laboratory. The new model, GAO078, demonstrated improved predictive ability over GEB052 and has had its predictions validated using cell line microarray data, as well as through laboratory-based experiments. The model also generated hypotheses utilizing cell death pathways and identified potential novel clinical use of approved chemotherapeutics.

Materials and methods

Predicting miRs targeting nodes in the GEB052 model. TargetScan (https://www.targetscan.org/vert_80/) and DIANA tools, (DIANA tools Software; microT-CDS v5.0; http://diana.imis.athena-innovation.gr) databases were used to predict miRs targeting the genes included in GEB052 (9). The DIANA software allows different threshold scores that can be set to 0.6, 0.9 and 0.99. The miRs that overlapped between conserved miR targets were identified through TargetScan and that from DIANA tools at three Target prediction scores (miTG score); the higher the miTG score the higher the probability of targeting (10,11). Conserved miRs from TargetScan were compared with miRs from DIANA tools at 0.99 score, and the overlapping miRs were selected for addition to the GEB052 model (Tables SI-III). A list of miRs from DIANA tools at 0.6, 0.9 and 0.99 scores is provided in Table SIV. Additional inclusion criteria included literature-based validation where nodes and miR-target interactions were identified based on luciferase reporter assay, reverse transcription-quantitative (RT-q) PCR and western blot methods. The interaction was included when two of these criteria were met. For the majority of excluded miRNAs no experimental validation was identified, except for three miRNA-target pairs: hsa-miR-128-3p-14-3-3 (RT-qPCR evidence only), hsa-miR-18a-5p-NCOA1 (luciferase validation only) and hsa-miR-9-5p-POU2F1 (luciferase validation only). The new model (GAO078) was visualized through Cytoscape (https://cytoscape.org) (12) with the genes, input, and outputs classed as model nodes whilst the relationships between the nodes were classed as edges. A schematic representation of the model construction and analysis is shown in Fig. SI.

GAO078 model analysis through CellNetAnalyzer. Following model construction, GAO078 was imported to CellNetAnalyzer CNA2025.1_87a for dependency matrix (DM) generation and logical steady state analysis (LSSA). DM analysis explores all signaling paths between every node in the model to every node in the model and can be conducted in both the full model ('wild-type') and in *in silico* knockout models. Through DM analysis, an overall dependency depicting the relationship from Node A to Node B is obtained. This leads to six different types of dependencies: no effect; strong activator; weak activator; strong inhibitor; weak inhibitor and ambivalent factor (9,13). Furthermore, dependencies in one simulation can be compared with another (such as a knockout scenario).

Comparatively, LSSA follows a signal through the network after defining a set of inputs such as GC ON and GR OFF. From this, LSSA indicates the overall activation state of each node with three possible node states [1 (ON), 0 (OFF) and NaN (undetermined)]. LSSA was conducted under the following simulation conditions:

i) Input GC is ON (1), GR is ON (1), and all miRs are ON (1), simulating wild-type GR/GC-sensitive cells and active miRs.
ii) Input GC is ON (1), GR is ON (1), and all miRs are OFF (0), simulating wild-type GR/GC-sensitive cells and inactive miRs.
iii) Input GC is ON (1), GR is OFF (0). and all miRs are ON (1), simulating mutant GR/GC-resistant cells and active miRs.
iv) Input GC is ON (1), GR is OFF (0), and all miRs are OFF (0), simulating mutant GR/GC-resistant cells and inactive miRs.

LSSA simulations also permitted comparison of node states between different simulations, which generated *in silico* predictions for how the gene/protein would be altered *in vivo*. Changes in node state between simulations were captured through E_{mod}. E_{mod} had three possible values in all cases: 1 (node is increased), 0 (node is unchanged) or -1 (node is decreased). A summary of how these E_{mod} values could be arrived at is summarized in Table SV.

GAO078 model validation. E_{exp} is a value that represents the change [upregulation (1), downregulation (-1), or unchanged (0)] in a given gene's expression from experimental data. E_{exp} values for the genes in the GAO078 model were retrieved from supplementary information from Bakker et al (9). Taking E_{mod} values from the analyses described above, the absolute value of E_{mod} - E_{exp} gave three possible outcomes for the model's prediction: 0 (correct); 1 (small error); and 2 (large error). Small errors represent a 'one-step' error (e.g. the model predicts it

is unchanged, but it goes up or down, or the model predicts it is up or down but it is actually unchanged). A large error is when the model predicted the opposite of what occurred experimentally.

Signal transduction score flow algorithm (STSFA). One limitation of LSSA is that analytical values are binary, that is ON or OFF, there is no proportionality or level of activation. One route to address this is the use of the STSFA, which is conducted in Cytoscape (14). STSFA enables the superimposition of microarray or ChIP-seq data onto a model to perform a more quantitative analysis (14). In this situation, quantitative analysis suggests that each node inside the model is given a 'score' to allow for comparison of relative activation/inhibition rather than a Boolean fixed state of 1 or 0 to denote ON or OFF. To perform STSFA analysis, each node in the model was given a starting score obtained from microarray data.

One complication to STSFA was that the miRs were not present in the microarray data. As such, four methods were developed and employed to identify the best way to represent microRNA signaling under STSFA, as shown in Table SVI. To statistically compare the four methods, one-way ANOVAs of the number of correct predictions, number of small error predictions, and number of large error predictions were performed. All four methods are indirect approximation approaches rather than efforts to reflect actual, measured values. While it is standard in computational biology to develop such novel approaches in the absence of suitable data, it should be noted that upstream values being, in some way, a function of other downstream values has precedent. For instance, the STSFA algorithm itself uses the downstream starting node scores to determine upstream edge weights (14). As such, though the mathematical innovation and implementation differs, the fundamental aspect of upstream elements being contingent on downstream nodes is previously established in the literature.

After removing all directly ambivalent relationships and running the algorithm, fold changes (FC) between resistant and sensitive node scores were determined, accompanied by Log_{10} of each fold change. A dynamic threshold was created based on the average Log_{10}FC +/- standard deviation (STDEV). This calculation was created for all four methods described in Table SVI. A node was considered upregulated when values were above the threshold and downregulated when values were below the threshold. Nodes whose Log_{10}FC fell within the threshold were deemed to be unchanged. For any node with a score of zero following STSFA, a manual calculation was performed to determine their score (as the STSFA algorithm does not introduce negative numbers as final values). The edge weights of the analysis were exported and the edge weights for all incoming reactions to the node of interest were summed alongside the starting score. This allowed for the representation of 'how negative' the node was. In cases where the node value for sensitive was negative whilst the resistant scenario was positive (or vice-versa) a fold change could not be calculated, and so the nodes were given a value of 'N/A' for their fold change and did not contribute to the dynamic threshold calculation. However, based on the directionality of which was positive, and which was negative, it was still possible to assign an E_{mod} of -1 or 1 to the node. For example, if the resistant simulation score was negative whilst the sensitive simulation was positive, the node was deemed downregulated in the resistant scenario and given an E_{mod} of -1. Similarly, if the resistant simulation score was positive whilst the sensitive simulation was negative, then the node was deemed to be upregulated in the resistant scenario and given an E_{mod} of 1.

Correct/small error/large error percentages for situations when the miRNAs are ON and OFF were calculated for both LSSA and STSFA. The mean, STDEV and P-value were calculated for the GEB052 and GAO078 (miRs OFF or ON). Correct prediction rates in the model were statistically validated in a similar manner to previous work (9), through the BINOM.DIST Excel function (binomial distribution probability) under a probability mass function setting, where the correct predictions were the number of successes, the total predictions assessed were the number of trials, and the chance of success was 1/3 (15). The chance of success being 1/3 was due to there being three possible outcomes for the ABS (E_{mod}- E_{exp}).

Cell lines. A total of three human leukemia cell lines were used in the present study: CEM-C7-14 and CEM-C1-15 were both gifts from E. Brad Thompson's laboratory (The University of Texas Medical Branch, Galveston, Texas 77550, USA) (16,17) and SUP-B15 (B-ALL) was from the American Type Culture Collection. Microscopic images for all cell lines are provided in Fig. S2. RPMI-1640 supplemented with 1% penicillin/streptomycin (BMG Labtech GmbH), 1% glutamine (BMG Labtech GmbH), and 10% FBS (Thermo Fisher Scientific, Inc.) was used for cell culture. Cells were maintained at 5% CO_2 and 37˚C. Dextran coated charcoal (DCC; HyClone; Cytiva) FBS was used in place of standard FBS when cells were treated with DEX (Enzo Life Sciences, Inc.) and dasatinib (DAS; MilliporeSigma). DCC FBS was added to eliminate other hormones that can interfere with the effect of DEX.

Tetrazolium compound 3-(4,5-dimethylthiazol-2-yl)-5-(3-carboxymethoxyphenyl)-2-(4-sulfophenyl)-2H-tetrazolium (MTS) assay. Cell viability was evaluated using the MTS assay. The MTS assay measures the mitochondrial activity of viable mammalian cells, which reduces the MTS tetrazolium molecule to produce a colored formazan dye (18). Cells (5,000 per well) were incubated at 37˚C for the indicated times with DEX, DAS and the combination and the viability of cells was measured using a FLUO star Omega (Omega Bio-Tek, Inc.) plate reader. Absorbance was detected at 490 nm (for the MTS product) and 690 nm (for background). The background was subtracted, and the values were normalized to the untreated control sample.

To determine if effects of drugs were additive, antagonistic or synergistic, Bliss analysis was employed (19-21). In a Bliss independence analysis, three different categories exist: the inhibition that is expected if the two drugs function independently is called expected inhibition. Observed inhibition is the actual inhibition for the drug combination as found through experiment. The synergy score (Observed - Expected) was the difference between the observed and expected inhibition. Positive score (>0) indicates synergy, zero score (=0) suggests additive interaction and negative score (<0) suggests antagonism.

Flow cytometry-cell cycle analysis. The effect of the investigated compounds on cell cycle progression was evaluated using fluorescence activated cell sorting (FACS) with propidium iodide (PI; MilliporeSigma). CEM-C1-15, CEM-C7-14 and SUP-B15 cells treated with DEX, DAS and DEX/DAS combination were prepared in 6-well plates at $1x10^6$ cell density and incubated for 48 h. Cells were then centrifuged at 3,300 x g for 5 min, at room temperature, after which the supernatant was removed, and the pellet was washed twice in 1 ml cold PBS and resuspended in 1 ml 70% cold ethanol for fixation on ice for at least 30 min. Cells were washed with PBS, after which 50 μl of RNase A solution was added, and cells were incubated for 15 min at room temperature. Cells were then washed again with PBS. 200 μl of PI solution was added per million cells and cells were kept at room temperature for 10 min before flow cytometry. BD FACS Symphony A1 (BD Biosciences) was used to acquire the samples, and BD FACS Diva® software (BD Biosciences) was used for analysis.

Samples were transferred to a 1.5 ml microcentrifuge tube and, using an adapter, introduced to the sample pin. A dot plot with Sides Scatter (SSC) on the vertical axis and Forward Scatter (FSC) on the horizontal axis and a histogram plot with Counts on the vertical axis and the PI-detecting Phycoerythrin (PE) fluorescent channel on the horizontal axis were generated. Single cells from unstained and stained untreated samples were analyzed through the 'preview' option and gated within an ellipse shape gate ('Cells/P1') to exclude doublets or debris. Flow cytometer settings were modified by adjusting photomultiplier tubes' voltages (PMTV; FSC-250, SSC-250 and PE-400) and data thereafter acquired. Cells from treated and PI positive samples were analyzed and the percentage parent (% Parent) values were taken as the percentage cell death. Flow cytometer acquisition settings were not changed throughout the acquisition of the same cell type. Acquisition data including % parent, total event count, and mean fluorescence intensity were collected at the end of the experiment and analyzed relative to the control. Exemplar dot plots of FACS gating are shown in Fig. S3.

Flow cytometry - annexin V-FITC (apoptosis) assay. The Annexin V-FITC labelling kit from (Thermo Fisher Scientific, Inc.) was used to identify phosphatidylserine on the cell membrane's outer surface in apoptotic cells (22). In a 6-well plate, CEM-C1-15, CEM-C7-14 and SUP-B15 were plated at a density of $2.5x10^5$ cells/ml. After 48 h of treatment with DEX, DAS and DEX/DAS combination, cells were collected and spun at 300 x g for 5 min at room temperature. The pellet was washed twice in cold PBS, and 195 μl of binding buffer with 5 μl of Annexin V-FITC was used to resuspend the cells. Cells were rinsed in 200 μl binding buffer after being incubated at RT for 10 min in the dark. Following that, 10 μl of the PI solution was added to cells that had been resuspended in 190 μl diluted binding buffer. BD FACS Symphony A1 (BD Biosciences) was used to acquire the samples, and BD FACS Diva® software (BD Biosciences) was used for analysis. For data acquisition, the procedure was identical to that described in the previous section, except that the VITC voltages were adjusted to 500. The sum of the percentages of early and late apoptotic cells is shown.

microRNA extraction and RT-qPCR analysis. CEM-C7-14, CEM-C1-15, and SUP-B15 cells were seeded in 6-well plates ($1x10^6$ cells/well) and treated with 1 μM DEX, 10 μM DAS or a combination. miRNA was isolated using the mirVana miRNA Isolation Kit (Thermo Fisher Scientific, Inc.), according to the manufacturer's instructions. Cells were washed with PBS and lysed in 600 μl Lysis/Binding Solution. The lysates were vortexed, mixed with miRNA Homogenate Additive, and incubated on ice for 10 min. An equal volume of Acid-Phenol was added, followed by mixing and centrifugation at 10,000 x g for 5 min at room temperature. The aqueous phase was transferred to a new tube and mixed with 1.25 volumes of 100% ethanol, then loaded onto the Filter Cartridge. The cartridge was washed with miRNA Wash Solution, followed by elution of RNA with 100 μl pre-heated Elution Solution. RNA was recovered by centrifugation at 16,000 x g for 20-30 sec and used for miRNA analysis. RNA concentration and purity were assessed using a Nanodrop 1000 Spectrophotometer (NanoDrop Technologies; Thermo Fisher Scientific, Inc.); samples with A260/280 ratios of ~2.0 were used for further analysis. cDNA synthesis was performed using the TaqMan Advanced miRNA cDNA Synthesis Kit (Thermo Fisher Scientific, Inc.), which involved poly(A) tailing, adaptor ligation, reverse transcription and amplification. TaqMan probes used for miRNA detection contained the FAM™ reporter fluorophore at the 5' end. Reverse transcription PCR was carried out using TaqMan Fast Advanced Master Mix and specific miRNA primers (Eurofins Scientific) with the universal reverse primer from Agilent Technologies. Each reaction (20 μl) included 10 μl master mix, 0.8 μl forward and reverse primers, 5 μl diluted cDNA and RNase-free water. All primers were ordered from Eurofins Company and listed in Table SVII. Reactions were run on a Rotor-Gene Q system (Qiagen GmbH), 3-step cycling was used. The cycling conditions consisted of 14 cycles of denaturation at 60˚C for 3 sec, followed by annealing/extension at 95˚C for 30 sec. The reaction was then terminated by a final step at 99˚C for 10 min. Each sample was analyzed in technical duplicates across three independent experiments. Ct values were automatically calculated using Rotor-Gene Q series software (Qiagen GmbH) (23).

U6 snRNA was selected as an endogenous reference control for normalization. Sequences of all miRs studied were from https://www.mirbase.org and are shown in Table SVIII. The forward primer for Human U6 snRNA is included in Table SVII. The reverse primer used was the Universal Reverse Primer from Agilent Technologies, Inc. (cat. no. 600037).

Statistical analysis. The statistical analysis and graphs were plotted using Excel (Microsoft Corporation) and GraphPad PRISM 10.2.0 (Dotmatics). One or two-way ANOVA (depending on the number of variables tested) followed by Tukey's multiple comparison tests was performed to assess the statistical significance of experiments. $P<0.05$ was considered to indicate a statistically significant difference.

Results

Model generation. Following the process described in the Materials and methods, Table I shows the miRs that were added to the GEB052 model to form the GAO078 model.

Table I. miR-node links.

miR	Node	PubMed ID	Method used
miR-152	YWHAB	25228695	Luciferase reporter assay, RT-qPCR and western blotting
miR-206	YWHAZ	27806334	Luciferase reporter assay, RT-qPCR and western blotting
miR-206	YWHAZ	30611620	Luciferase reporter assay, RT-qPCR and western blotting
miR-200c	YWHAG	25798844	Luciferase reporter assay, RT-qPCR and western blotting
miR-200 and 141	YWHAG	30613263	Luciferase reporter assay, RT-qPCR and western blotting
miR-155	FOS	30898623	RT-qPCR and western blotting
miR-155	RELA	30497068	Luciferase reporter assay, RT-qPCR and western blotting
miR-10a	NCOR2	30680848	Luciferase reporter assay, and western blot
miR-10a and b	NCOR2	21212796	Luciferase reporter assay, RT-qPCR and western blotting
miR-27b	NR2F2	27844448	Luciferase reporter assay, RT-qPCR and western blotting
miR-132	EP300	26686902	Luciferase reporter assay, RT-qPCR and western blotting
miR-133b	SUMO1	34918563	Luciferase reporter assay, RT-qPCR and western blotting
miR-194	SUMO2	30232383	RT-qPCR and western blotting
miR-20a	ABCA1	28602962	Luciferase reporter assay, RT-qPCR
miR-27b	ABCA1	26520906	Luciferase reporter assay, RT-qPCR and western blotting
miR-33a	ABCA1	25329888	RT-qPCR and western blotting
miR-33	ABCA1	27471270	RT-qPCR and western blotting
miR-33b	ABCA1	31409515	RT-qPCR and western blotting
miR-106b	ABCA1	22119192	Luciferase reporter assay, RT-qPCR and western blotting
miR-144	ABCA1	24733347	Luciferase reporter assay, RT-qPCR and western blotting
miR-10b	CREB1	26796749	Luciferase reporter assay, RT-qPCR and western blotting
miR-27b	CREB1	27809310	Luciferase reporter assay, RT-qPCR and western blotting
miR-27a	CREB1	29089199	Luciferase reporter assay, RT-qPCR and western blotting
miR-494	LIF	20837890	Luciferase reporter assay, RT-qPCR and western blotting
miR- 137	NCOA2	26461474	Luciferase reporter assay, RT-qPCR and western blotting
miR-20a and 106	NCOA3	25634356	RT-qPCR and western blotting
miR- 137	NCOA3	26066330	RT-qPCR and western blotting
miR-9	POU2F1	27658774	Luciferase reporter assay, and RT-qPCR
miR-134	CREB1	31625272	RT-qPCR and western blotting
miR-10a	CREB1	27292126	RT-qPCR and western blotting
miR-182	MED1	30160993	Luciferase reporter assay, RT-qPCR and western blotting
miR-655	POU2F1	31799644	Luciferase reporter assay, RT-qPCR and western blotting

Column 1 shows the microRNA, Column 2 shows the node it targets, and Column 3 shows the PubMed ID evidence of a paper supporting the interaction. Column 4 details the methods used. ABCA1, ATP binding cassette subfamily A member 1; CREB1, CAMP responsive element binding protein 1; EP300, EP300 lysine acetyltransferase; FOS, Fos proto-oncogene, AP-1 transcription factor subunit; LIF, LIF interleukin 6 family cytokine; MED1, Mediator complex subunit 1; miR, microRNA; NCOA2, Nuclear receptor coactivator 2; NCOA3, Nuclear receptor coactivator 3; NCOR2, Nuclear receptor corepressor 2; NR2F2, Nuclear receptor subfamily 2 group F member 2; POU2F1, POU class 2 homeobox 1; RELA, RELA proto-oncogene, NF-kB subunit; RT-qPCR, reverse transcription-quantitative PCR; SUMO1, Small ubiquitin like modifier 1; SUMO2, Small ubiquitin like modifier 2; YWHAB, Tyrosine 3-monooxygenase/tryptophan 5-monooxygenase activation protein beta; YWHAG, Tyrosine 3-monooxygenase/tryptophan 5-monooxygenase activation protein gamma; YWHAZ, Tyrosine 3-monooxygenase/tryptophan 5-monooxygenase activation protein zeta.

Notably, as shown in Table SI, some microRNAs targeted individual genes that were part of a larger aggregate node in the model (e.g. nodes 14-3-3 contain YHWAB, YHWAZ and YHWAG among others). The final GAO078 is shown in Fig. 1.

The GAO078 model consists of 78 nodes and 274 interactions, which includes 52 nodes and 241 interactions from the GEB052 model and 26 new miRs (Fig. 1A). Furthermore, the network is connected to one input node, which is the GC and two output nodes representing inflammation and cell death. In this model, nodes represent genes, proteins and miRs that interact with GR as well as the input (GC) and outputs (cell death and inflammation) whilst the edges represent the stimulatory or inhibitory interactions between the nodes.

Dependency analysis of GAO078 model. As described in the Methods, DM analysis permits identification of the overall relationship between each node in the model with each node in the model. Additionally, comparison of the DM from one

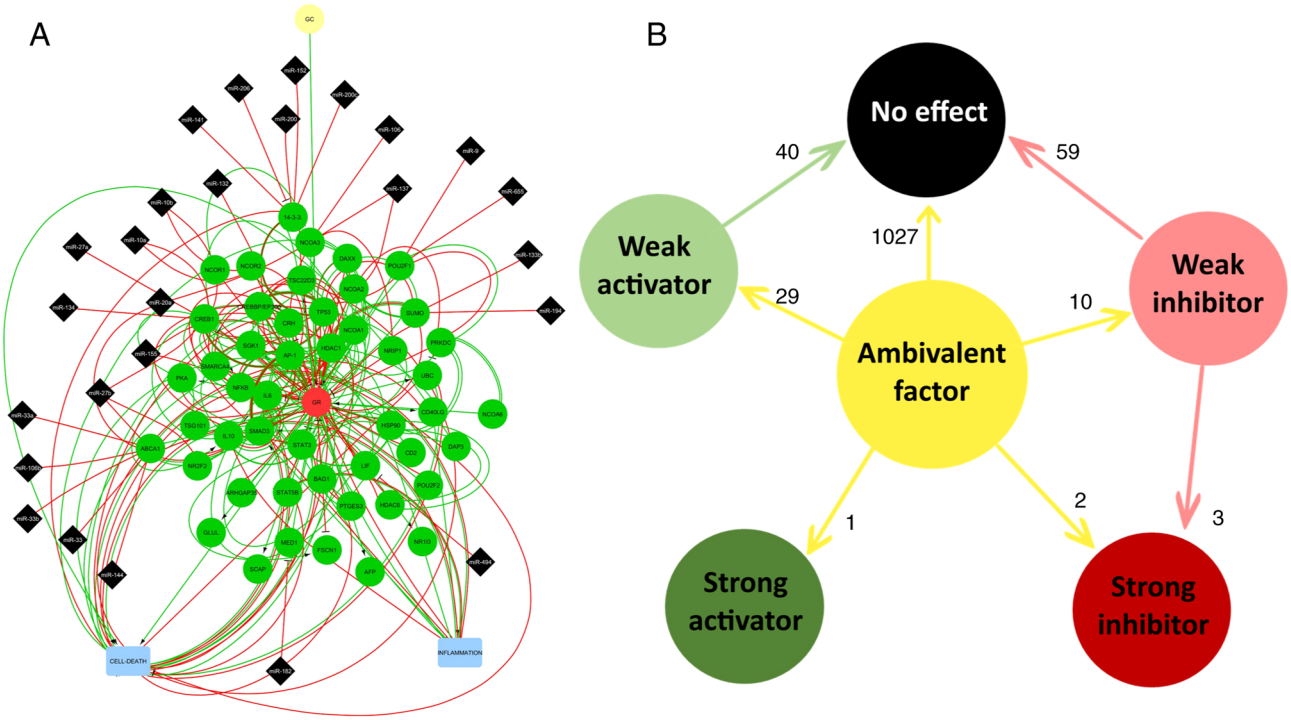


Figure 1. The GAO078 model. (A) The GAO078 model, containing 78 nodes with 274 interactions as visualized using Cytoscape. The central node (GR) is shown as a red circle; GC is shown in yellow circle; other genes are shown in green circles; Cell Death and Inflammation outputs are indicated in blue squares and miRs are shown as black diamonds. Green arrows represent activating interactions, whilst inhibitory interactions are shown as red. (B) DM changes of the GAO078 model after an *in silico* GR knockdown. The figure also illustrates how dependencies changed once the GR node was eliminated from the GAO078 model. Weak activators and inhibitors are shown by light green and pink circles, respectively, whilst ambivalent dependencies are shown by a yellow circle. Strong activators are represented by the dark green circle, and strong inhibitors are represented by the dark red circle. The dark grey circle indicates that there are no effect dependencies. Arrows show the number of dependencies that changed from one type to the other.

simulation to the DM of another can help illustrate changes to biological relationships following, for instance, gene knockout. DM of the wild-type GAO078 model shows a total of 6,084 (78x78) dependencies, of which 3,130 (51.45%) are no effect, 2,800 (46.02%) are ambivalent, 87 (1.43%) are weak inhibitor, 63 (1.04%) are weak activator, 2 (0.03%) are strong inhibitor and 2 (0.03%) are strong activator (Fig. S4). A large number of ambivalent factors result from the complex relations between nodes, which are influenced by the positive and negative feedback loops and their paths (24). For the GR knockout model, a total of 5,929 (77x77) dependencies were identified, out of which 4,211 (71.02%) were no effect, while 1,641 (27.68%) were ambivalent. There were 29 (0.49%) and 38 (0.64%) weak inhibitors and weak activators respectively, whilst there were 7 strong inhibitors (0.12%) and 3 strong activators (0.05%). Dependency changes following GR knockout are shown in Fig. 1B. Changes to strong activators or strong inhibitors are those most likely to show an effect *in vivo*. DAP3 from ambivalent in the wild-type simulations became a strong activator of CELL-DEATH in GR mutant scenario, whereas STAT5B under the same conditions became a strong inhibitor of CELL-DEATH. Table II shows the relationships that change to strong activator and strong inhibitor following GR knockout (KO).

As the dependency change between STAT5B and CELL-DEATH following GR knockout is a key outcome of the model, this was further investigated. Feedback loops are essential for network integrity, and this can be seen by comparing the wild-type GAO078 model to the GR knockout model. The full (wild-type) GAO078 model had a total of 512,060 feedback loops. Limited to 2-step feedback loops, there were 64 feedback loops present, consistent with the original GEB052 model (9). When GR is knocked out, only 2,990 feedback loops in total remain, of which 38 are two-step feedback loops. The underpinning literature behind CellNetAnalyzer highlights feedback loops as a key determinant of whether dependency matrix relationships are strong/total activators/inhibitors or weak/non-total activators/inhibitors (13).

In terms of the relationship between STAT5B and CELL-DEATH specifically, CNA 2026.1 was used for pathway tracing between these two nodes. In the wild-type model, 438,960 paths were present between STAT5B and CELL-DEATH, of which 219,479 were negative modes and 219,481 were positive. This represents the balance of positive and negative paths between the two nodes, reflective of the original ambivalent dependency. Comparatively, in the mutant (GR KO) model, there was only one path present from STAT5B and CELL-DEATH, which was the direct inhibitory relationship. This validated the importance of the GR to the network, provided direct evidence for the magnitude of effect from STAT5B to CELL-DEATH and validated the importance of feedback loops and interconnectivity in model structure.

Complementing DM analysis is LSSA, which allows capturing of the total activation state of the node (ON, OFF, undetermined) after upstream inputs. At the start of the LSSA, a value of NaN (undetermined) is given for each node, other

Table II. Changes to strong inhibitors and strong activators following GR Knockout.

Node A	Node B	WT Dependency	KO Dependency
STAT5B	CELL-DEATH	Ambivalent	Strong inhibitor
MiR27B	NR2F2	Ambivalent	Strong inhibitor
MiR182	MED1	Weak inhibitor	Strong inhibitor
MiR655	POU2F1	Weak inhibitor	Strong inhibitor
MiR9	POU2F1	Weak inhibitor	Strong inhibitor
DAP3	CELL-DEATH	Ambivalent	Strong activator

DAP3, Death associated protein 3; GR, glucocorticoid receptor; KO, knockout; MED1, Mediator complex subunit 1; NR2F2, Nuclear receptor subfamily 2 group F member 2; POU2F1, POU class 2 homeobox 1; STAT5B, Signal transducer and activator of transcription 5B; WT, wild type.

than the input node, which is manually modified. After setting inputs, the signal flows through the model's edges until each node reaches a 'steady state' (ON, OFF or NaN). LSSA input settings were described in the Methods, and as aforementioned E_{mod} was calculated. E_{mod} could take three possible values: 1 indicates upregulation in the mutated scenario relative to the wild type; 0 suggests no change; -1 indicates the model predicts downregulation in the mutant scenario. E_{mod} values for simulations are shown in Tables SIX and SX. In a GR WT scenario compared with a GR mutant scenario where miRs are ON, there are three upregulated genes (SUMO, DAXX and HDAC1), while these genes were unchanged after miRs are OFF. In a GR WT scenario compared with a GR mutant scenario, when miRs are ON, two genes (MED1 and NR2F2) were uniquely downregulated, and these genes are unchanged when miRs are OFF. The other nodes have the same prediction in both miRs ON and OFF scenarios, after GR WT is compared with the GR mutant scenario (Tables SXI and SXII).

GAO078 model validation. To assess the accuracy of the model more broadly, E_{exp} values, which show the change in the gene's expression levels from experimental data, were taken from Bakker *et al* (9) and used in conjunction with E_{mod} to validate GAO078 model predictions. The original microarray data used for the comparison between GC-sensitive and GC-resistant cell lines were collected from the Gene Expression Omnibus database (https://www.ncbi.nlm.nih.gov/geo/). For each comparison, the E_{exp} values were retrieved from Bakker *et al* (9) and compared with the model predictions (E_{mod}).

The summary is illustrated as a percentage for each comparison and is demonstrated, as described in the Methods, as correct/small error/large error for scenarios when the miRs are ON and OFF. Graphs show correct/small error/large error for scenarios when the miRs are ON and OFF (Fig. 2). The comparison shows no difference between the original GEB052 and GAO078 when the miRs are ON. Statistical analysis demonstrated $P<0.05$ for improved predictive power for GAO078 when miRNAs were OFF.

Comparison of GAO078 model predictions between LSSA and STSFA simulations. *In silico* predictions using the score flow algorithm were developed and compared with experimental gene expression profiles to assess the STSFA network's genome-wide predictive power more quantitatively. Distributions of correct predictions, small errors and large errors, were compared under all studied circumstances and the majority of the genes were correctly predicted by the STSFA model between the resistant and sensitive simulations. Each miR in the model was scored using one of four methods as described in the Methods. The correct prediction rate for all four methods across all six comparisons ranged between 70.00-82.50%, whilst small errors ranged between 17.50-30.00 and 0.00-2.50% represented the large error range (Fig. S5A). Values for all four methods in comparison 1 ranged from 71.79% to 75% for correct, 25% to 28.21% for small error and were 0 for large error predictions (Fig. S5Aa); in comparison 2 values ranged from 79.49% to 80% for correct, 20% to 20.51% for small error and were 0 for large error predictions (Fig. S5Ab); in comparison 3 values ranged from 79.49% to 82.50% for correct, 17.50% to 20.51% for small error and were 0 for large error predictions (Fig. S5Ac); in comparison 4 values ranged from 70% to 76.92% for correct, 23.08% to 30% for small error and were 0 for large error predictions (Fig. S5Ad); in comparison 5 values ranged from 71.05% to 75% for correct, 22.50% to 28.95% for small error and from 0% to 2.50% for large error predictions (Fig. S5Ae); in comparison 6 values ranged from 71.05% to 77.50% for correct, 22.50% to 28.95% for small error and were 0% for large error predictions (Fig. S5Af). The average of correct percentage, small and large errors using four methods is shown in Fig. S5B. In addition, due to the novelty of this microRNA scoring approach in the use of STSFA, one-way ANOVAs were performed as described in the Methods to compare the four methods. This was against the number of correct predictions, the number of small error predictions and the number of larger error predictions. P-values for these ANOVAs were 0.229, 0.887 and 0.582 respectively, indicating that the four different approaches are equally powerful.

STSFA semi-quantitative analysis resulted in more accurate prediction results than LSSA analysis, consistent with previous literature (9). Fig. 2B demonstrates the percentage of correct, small and large error predictions when LSSA compared with STSFA methods were used to analyze GAO078 model accuracy over microarray source data. The correct prediction rate of the GAO078 model calculated

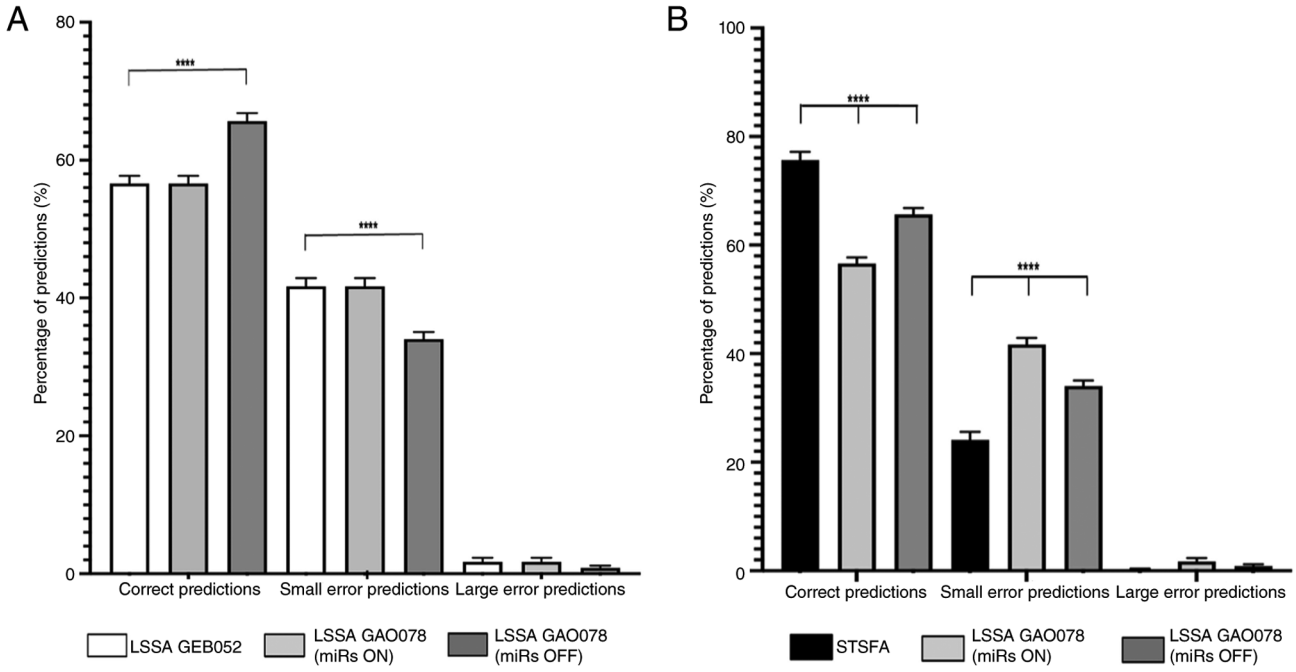


Figure 2. GEB052 LSSA vs. GAO078 LSSA and STSFA analysis. (A) Comparison of LSSA simulations in GEB052 vs. GAO078 models. Correct, small and large error predictions from LSSA for scenarios when the miRs are ON and OFF were compared with the original LSSA predictions for the GEB052 model. (B) Comparison between the prediction rates of LSSA (miRs ON and OFF) and STSFA for the GAO078 model. Correct, small and large error predictions from LSSA for scenarios when the miRs are ON and OFF were compared with the STSFA GAO078 model. Statistical analysis was performed using two-way ANOVA followed by Tukey's multiple comparison tests. Error bars represent SEM. ****P<0.0001 vs. GEB052 as a control. LSSA, logical steady state analysis; STSFA, signal transduction score flow algorithm; miR, microRNA.

using STSFA was 75.7% compared with LSSA [miRs OFF (65.63%) and miRs ON (56.6%)]. In summary, the STSFA approach produced a markedly high percentage of accurate (correct) predictions and indicates that the model predictions were closer to the experimental data.

Finding drugs targeting nodes identified by model simulations. The loss of GR in model simulations led STAT5B to become a strong inhibitor of CELL-DEATH (from an ambivalent factor), suggesting it to be a valuable candidate for drug targeting in GR-resistant cells. DRUGSURV analysis (http://www.bioprofiling.de/drugsurv; accessed 2019) (25) suggested that dasatinib (DAS), an approved drug used in CML therapy for its ability to target BCR-ABL, targeted STAT5B. Thus, DAS was used to treat leukemia cells to validate GAO078 model predictions.

Dexamethasone and dasatinib effects on the viability of ALL cell lines. To validate the GAO078 model, the effect of DEX and DAS on ALL cells was analyzed. The experiment was carried out to establish the best experimental conditions to study cytotoxicity of DEX, DAS and the combination of both drugs on the CEM-C7-14, CEM-C1-15 and SUP-B15 cell lines *in vitro* using an MTS assay, with increasing concentrations ranging from 10 nM to 1 μM DEX and from 400 nM to 50 μM DAS either alone or in combination for 48 h (Fig. 3) or ranging from 100 nM to 10 μM DAS alone for 48 h [Fig. S6A i), iii) and v)] or for 72 h [Fig. S6B i), iii) and v)] or in combination with increasing concentrations of DEX ranging from 10 nM to 1 μM for 48 h [Fig. S6A (ii), iv) and vi) A] or for 72 h [Fig. S6B (ii), iv) and vi)]. After 48 h of treatment the viability of cells was reduced after treatment with DEX and DAS and cell death was markedly increased in the cell lines studied when incubated with DEX and DAS (Fig. 3).

As shown in Fig. 3A, the highest concentration of DEX used was 1 μM, and the lowest was 0.01 μM. Results show a significant reduction in the viability of CEM-C7-14 cells at 0.01 μM to 61 and 34% at maximum (1 μM) DEX concentration over 48 h. CEM-C1-15 and SUP-B15 cells were incubated with the same concentrations of DEX for 48 h. CEM-C1-15 viability at 0.01 μM was reduced to 92% and at 1 μM to 82.3%, however this was not significant. SUP-B15 cells viability showed a slight reduction to 83% at lowest concentration (0.01 μM) and 70% at the highest concentration (1 μM) for 48 h (Fig. 3A).

DAS cytotoxicity was also assessed; ALL cell lines were incubated with DAS at increasing concentrations from 100 nM up to 50 μM (Fig. 3B and Fig. S6). Cell viability of CEM-C7-14 and CEM-C1-15 cells was mostly unchanged at lowest concentrations, and decreased at the highest concentrations (50, 25, 12.5 and 10 μM), with CEM-C1-15 having a slightly stronger response than CEM-C7-14 (19% at 50 μM for CEM-C7-14 and 17% for CEM-C1-15 at 50 μM, Fig. 3B). Cell viability of SUP-B15 decreased gradually from the lowest concentration of 100 nM (around 80%, although not significant) with further decreases to 23% at 50 μM (Figs. 3B and S6). Longer incubations with DAS did not make substantial difference in viability of cell lines tested (Fig. S6).

Subsequently, all cell lines were treated with a combination of serial dilutions from 1 μM DEX maximum dose and 50 μM DAS maximum dose over 48 h (Fig. 3C and Fig. S6). In CEM-C7-14, the cytotoxic effect of both drugs combined was observed. At the highest dose of 50 μM DAS and 1 μM DEX,

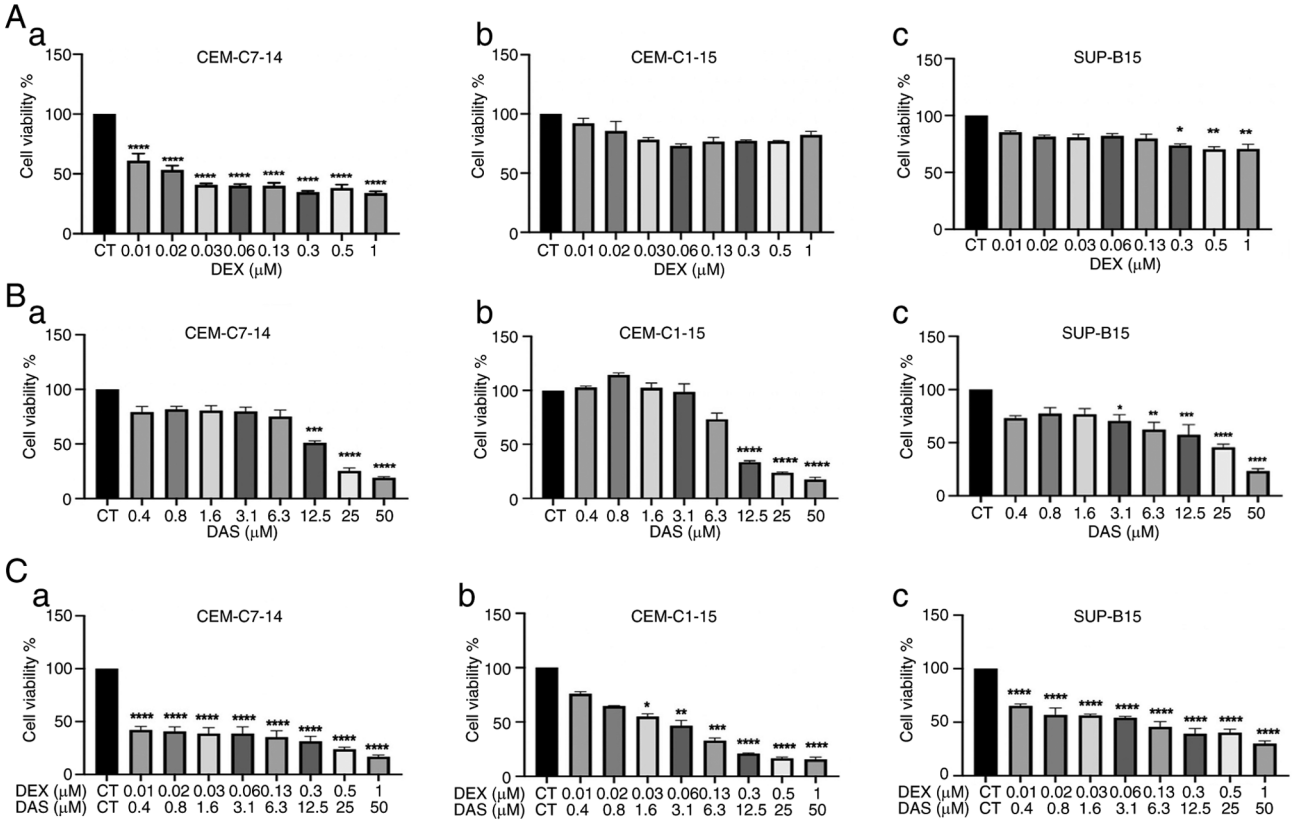


Figure 3. Viability of leukemia cells treated with DEX, DAS and combination. (A) (a) CEM-C7-14, (b) CEM-C1-15 and (c) SUP-B15 cells were treated with DEX serially diluted from a maximum dose of 1 μM; (B) (a) CEM-C7-14, (b) CEM-C1-15 and (c) SUP-B15 cells were treated with DAS serially diluted from a maximum dose of 50 μM and (C) (a) CEM-C7-14, (b) CEM-C1-15 and (c) SUP-B15 cells were treated with DEX and DAS combination, over 48 h and viability was determined using the MTS assay. The graphs represent three independent experiments. Statistical analysis was performed using one-way ANOVA followed by Tukey's multiple comparison tests. Error bars represent SEM. *P<0.05, **P<0.01, ***P<0.001 and ****P<0.0001 vs. CT. Data labels show rounded values. DEX, dexamethasone; DAS, dasatinib; MTS, tetrazolium compound 3-(4,5-dimethylthiazol-2-yl)-5-(3-carboxymethoxyphenyl)-2 (4-sulfophenyl)-2H-tetrazolium; CT, control.

the result revealed 17% cell viability, whereas cell viability of ~40% was observed with the lowest drug concentration (starting with 0.1 μM DAS and 0.01 μM DEX) (Figs. 3C and S6). CEM-C1-15 cells were also incubated with the DEX/DAS drug combinations, resulting in 15.8% of cell viability at 50 μM DAS and 1 μM DEX and ~70%, non-significant changes in cell viability at the lowest concentrations (0.1, 0.2 μM DAS and 0.01, 0.02 μM DEX; Figs. 3C and S6). SUP-B15 cell viability at a maximum dose (50 μM DAS and 1 μM DEX) of drugs was 30%, and at a minimum dose 71% (0.1 μM DAS and 0.01 μM DEX; Figs. 3C and S6). 72 h treatment duration showed similar results to 48 h treatment in all cell lines (Fig. S6). In conclusion, CEM-C7-14 cells were more sensitive to DEX. In comparison with the relatively GC-resistant CEM-C1-15, SUP-B15 exhibited mild cytotoxicity with 1 μM DEX. DAS mostly affected SUP-B15 cells and additionally, combination treatments enhanced cytotoxicity effects in all three cell lines when compared with the single drug treatment.

To assess if the effect of combining DEX and DAS was categorized as additive, synergistic, or antagonistic, the Bliss independence model was used in three cell lines (CEM-C7-15, CEM-C1-14 and SUP-B15; Table SXIII; Fig. S7). Bliss independence analysis demonstrated synergistic interaction between DEX and DAS across all tested concentration combinations. Observed inhibition consistently exceeded Bliss-predicted additive effects, providing positive synergy scores throughout the experiment in all 3 cell lines. No antagonistic interactions were observed. These findings indicated a synergistic interaction between DEX and DAS, with the strongest effect occurring at intermediate dose combinations. The combination generally produced inhibition exceeding Bliss model predictions, consistent with predominantly synergistic interactions, although the degree of synergy varied with drug concentration and cell line.

Flow cytometry analysis of leukemia cells treated with DEX and DAS. To consolidate these findings by providing another method to determine cell viability, PI staining followed by flow cytometry was performed (Fig. 4). Data revealed that the strongest increase in the Sub-G_1 population was observed in the DEX-treated CEM-C7-14 cell line, followed by SUP-B15 cells; although there was a statistically significant increase in DEX-treated CEM-C1-15 cells, this effect was smaller (Fig. 4A compare DEX bars with CT bars). In all leukemia cell lines treated with DAS and the combination, there was a significant increase in the Sub-G_1 phase when compared with the control. When both drugs were combined, the percentages increased even further, with the strongest effect shown in CEM-C1-15 cells (compare grey bars to black and white bars across Fig. 4A). This indicated that combined treatment has the most cytotoxic effect in leukemia that is less sensitive to DEX.

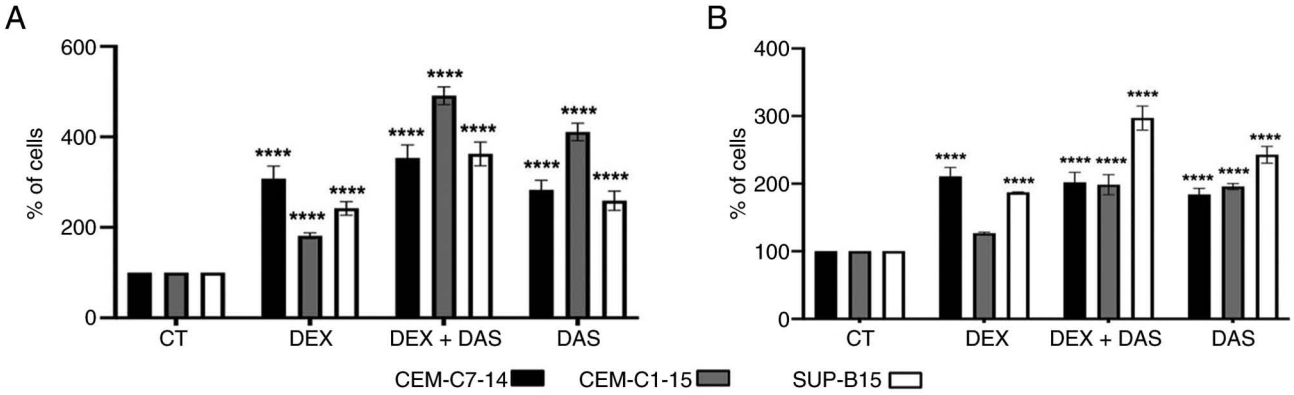


Figure 4. DEX and DAS affect ALL cell fate. (A) Sub-G_1 cell cycle phase and (B) Annexin V-mediated apoptosis percentages of CEM-C7-14, CEM-C1-15 and SUP-B15 cells treated with 1 μM DEX, 10 μM DAS and DEX/DAS combination over 48 h measured by flow cytometry with PI and Annexin V assay, respectively. The graphs represent three independent experiments. Statistical analysis was performed using two-way ANOVA followed by Tukey's multiple comparison tests. Error bars represent SEM. ****P<0.0001 vs. CT. DEX, dexamethasone; DAS, dasatinib; ALL, acute lymphoblastic leukemia; CT, control.

Additionally, to determine the type of cell death taking place, Annexin V assay was employed to measure apoptosis. The percentage of apoptotic CEM-C7-14 and SUP-B15 cells increased when cells were treated with DEX, DAS and in combination treatment and this effect was statistically significant (Fig. 4B; compare black and white bars in treated samples to control), whereas an increase in CEM-C1-15 was not statistically significant (Fig. 4B; compare grey bars in DEX-treated cells to control). The highest level of apoptosis was detected in DEX and DAS-treated SUP-B15 cell lines (Fig. 4B; compare white bars to respective controls in DAS and combination-treated cells). These results indicated that DEX elicits its cytotoxic effect in CEM-C7-14 and potentially in SUP-B15 cells mostly through the apoptotic pathway, as overall cell death measured through Sub-G_1 and apoptotic cell death measured through Annexin V assay were similar. However, in CEM-C1-15 cells DEX increased overall cell death but the increase in apoptotic cell death was not significant (Fig. 4B). Effects of DAS and combined treatment are more complex and show differential effects depending on the cell line. In conclusion, cell death either measured generally via Sub-G_1 or measuring apoptosis specifically increases markedly in the presence of DEX, DAS and combination in leukemia cell lines, however, this effect is differential and depends on the cell death type and the cell line investigated.

Analysis of micro-RNA expression in ALL cell lines. The GAO078 model predicted that three miRs (miR-27a, miR-20a and miR-9) target a high number of nodes in the model (Tables SXIV and SXV). Note that miRs overlapping between TargetScan (conserved) and DIANA tools, regardless of experimental validation, were used to identify nodes targeted by the same miRs and nodes most frequently targeted by different miRs (Table SXIV). In addition, according to previous literature, miR-27a and miR-20a were considered good prognostic factors, while miR-9 was a bad prognostic factor in the response to leukemia therapy (Tables SXVI and SXVII) (26). Therefore, these three miRs were chosen for further study and their expression was investigated in all ALL-cell lines treated with DEX+DAS using RT-qPCR.

Results shown in Fig. 5 indicated that in CEM-C7-14 cells treated individually with DEX or DAS there was no significant effect on the expression of miR-27a, miR-20a or miR-9, whereas DEX/DAS combined treatment resulted in substantial upregulation of miR-20a. MiR-27a and miR-9 expression levels increased markedly in DEX-treated CEM-C1-15 cells and miR-20a expression was markedly upregulated in CEM-C1-15 when treated with DAS or DEX/DAS combination. MiR-9 expression was found to be markedly upregulated in DEX or DAS treated CEM-C1-15 cells individually or in combination. The expression levels of all three miRs increased in SUP-B15 cells treated with DAS, whilst miR-9 expression levels increased in SUP-B15 cells treated with the combination of DEX/DAS. Experiments using miRNA mimic/inhibitor, antagomirs and rescue experiments were not performed and are planned for future investigations.

Discussion

Systems biology was used to increase understanding of GR signaling in ALL, aiming to uncover the causes of resistance and reveal potential ways to increase sensitivity of leukemia cells to GC treatment. The GAO078 model was built by adding miRs to the previous GEB052 model to investigate the importance of miRs in ALL progression and chemoresistance. Simulations indicated increased predictive capacity of the GAO078 model compared with GEB052, which was further tested *in vitro*. The models facilitated the identification of DAS as a potential drug to be used in the treatment of ALL. Cytotoxicity assays confirmed that, in certain experimental conditions, DAS in the presence of DEX exerts increased cytotoxicity for some of the ALL-cell lines studied, therefore partially validating model predictions.

A complex and important relationship between miRs and GR function is suggested by the results obtained using TargetScan and DIANA databases. For each node, the conserved site number was between 0-145, whereas the poorly conserved ranged between 16-4284 (Tables SI and SII). MiRs that overlapped between TargetScan (conserved) and DIANA tools, irrespective of experimental validation, were used to identify the nodes most frequently targeted by miRs. This investigation suggested that 85 miRs target the transcription

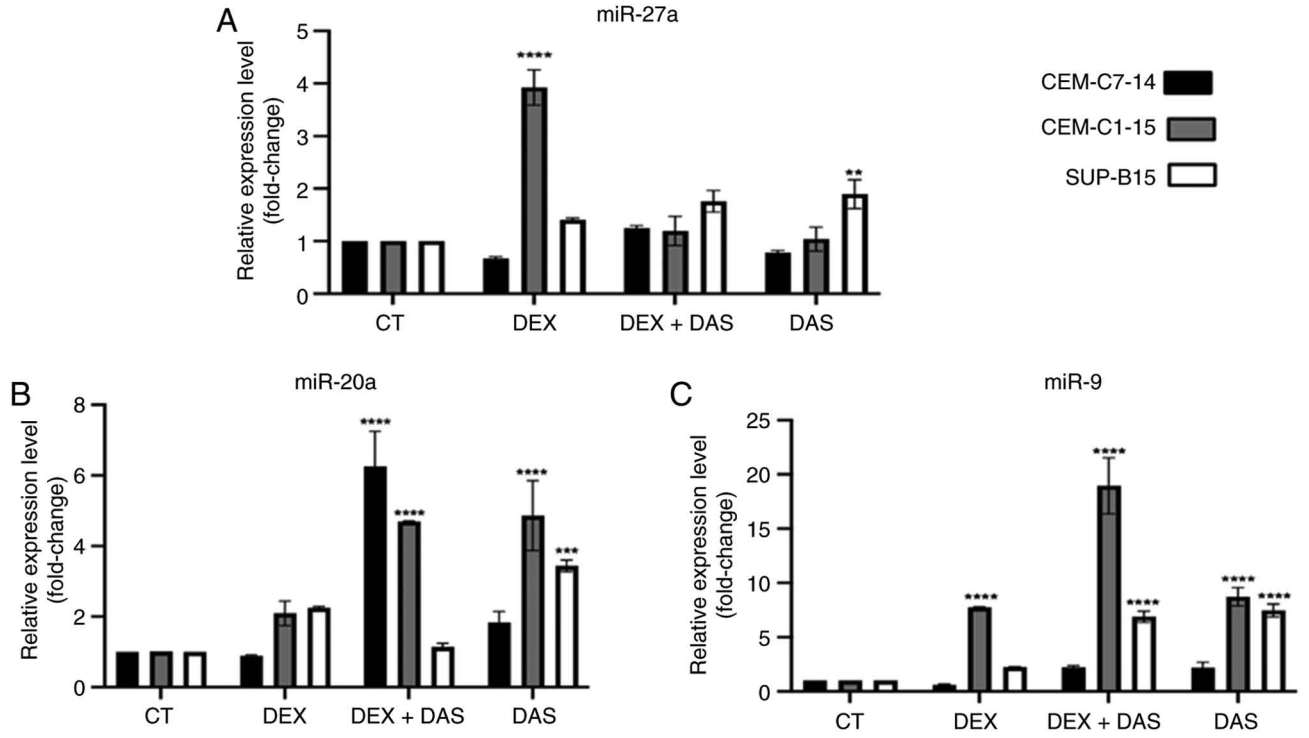


Figure 5. miR-27a, miR-20a and miR-9 expression. The level of (A) miR-27a, (B) miR-20a and (C) miR-9 gene expression in all ALL-cell lines treated with 1 μM DEX, 10 μM DAS and in combination over 24 h, determined by RT-qPCR. The graphs represent three independent experiments. Statistical analysis was performed using two-way ANOVA followed by Tukey's multiple comparison tests. Error bars represent SEM. **P<0.01, ***P<0.001 and ****P<0.0001 vs. CT. miR, microRNA; ALL, acute lymphoblastic leukemia; DEX, dexamethasone; DAS, dasatinib; RT-qPCR, reverse transcription-quantitative PCR; CT, control.

factor cAMP responsive element binding protein 1. A total of 68 miRs target the ATP-binding cassette transporter A1, which belongs to a family of proteins linked to drug resistance that function to pump drugs out of cells (27) (Table SII).

Although it would have been possible to add a much wider range of miRs to the model, during the addition process it was deemed that a careful balance was needed between capturing important regulators and avoiding false positives. At the time of the addition, the majority of the evidence papers studying miRs did so through RT-qPCR, western blotting, or luciferase to validate the miR-target link. Requiring a prospective miR to have at least two out of the three primary methods evidenced in the literature was considered to be a good balance between the two considerations listed above. It is possible, however, that the model could be developed further still, through the inclusion of more miRs.

Multiple changes to strong activators or inhibitors were seen in the model following GR KO; for instance, DAP3 and STAT5B. These alterations may have implications *in vivo* due to a lack of feedback loops, therefore leading to a strong effect. The strength of the model was further confirmed through LSSA, which had an average correct prediction rate of 65.63% (P<0.01) and improvements were further seen through STSFA, due to its semi-quantitative nature and addition of weights to each edge based on microarray data. STSFA led to the majority of the genes being correctly predicted (70.00-82.50%), thus providing additional validation that its predictions are markedly more accurate than LSSA. This is in line with earlier research using the STSFA to analyze the TP53 model, which demonstrated that the STSFA produced more accurate predictions with a correct rate of 77% (28).

The higher predictive rate of the GAO078 model compared with the previous GEB052 model provides improved, more useful information that could signpost its use as a potential prognostic tool for facilitating the development of personalized anti-cancer treatments. Furthermore, this method, upon further testing, could help in predicting how each patient will respond to therapy and identifying the most effective treatment plans as the disease progresses. Although the model demonstrates high predictive capacity, it is nonetheless limited by its Boolean, surface-level perspective of the biological networks it captures. Nuances, such as physiological RNA and protein levels, as well as wider regulatory elements that are not captured, are missed in this model. Thus, future iterations of the model could endeavor to incorporate greater depth of information, which will permit a more quantitative view, including sensitivity analysis.

Glucocorticoids are part of the conventional treatment for ALL (29). Even though most ALL patients who receive standard-of-care treatment undergo remission, a small percentage of individuals relapse and have a poor prognosis (30). Additionally, medication resistance and the toxicity of medicines continue to be major issues. To validate GAO078 model predictions, MTS and FACS were carried out using synthetic glucocorticoid DEX and kinase inhibitor DAS. A range of concentrations of DAS (from 100-50 μM) and DEX (from 10 nM-1 μM) was tested (Figs. 3 and S6). Cell death was stimulated in CEM-C7-14 cells following 48 h DEX treatment, but that was not the case for CEM-C1-15 cells. DEX exerted cytotoxic effects on the B-ALL cell line SUP-B15 in accordance with previously published reports (31), which is of note as other cell lines in the present study were T-cell acute lymphoblastic leukemia. The FDA has approved imatinib and DAS for the

treatment of patients with Philadelphia chromosome-positive ALL. Tyrosine kinase inhibitors, along with cytotoxic medications, are currently the first line of treatment (32).

The DAS/DEX combination treatment had small effects in the DEX-sensitive leukemia cells, although synergistic effects of two drugs were observed across all cell lines studied. In CEM-C1-15 and SUP-B-15 leukemia cells, the effects of DAS were cell-type dependent. A similar response to DEX/DAS treatment was observed in the BCR-ABL positive SUP-B15 cells and the BCR-ABL negative CEM-C1-15 cell lines, suggesting that DAS, upon further testing, could be considered as a potential treatment of DEX-resistant leukemia irrespective of BCR-ABL status, although this conclusion is limited by use of only one BCR-ABL negative and one BCR-ABL positive cell line. Although limited, the results obtained by MTS and FACS assays (Sub-G_1 and Annexin V), suggested that in addition to apoptosis, other alternative types of cell death could be a basis for the explanation of these results (33). These results could also be due to methodological differences in MTS and FACS assays. Future investigations should shed more light on the molecular aspects of this observation.

Analysis of DEX/DAS treatment on miR-27a, miR-20a and miR-9 showed that in several cases there was an increase in the expression of these miRs. Given that all three miRs are predicted to target nuclear receptor coactivators as well as nuclear receptor corepressors, the final outcome on nuclear receptor function could be a balance between multiple, complex networks. Experiments to manipulate miRNA levels using antagomirs/mimics were not performed, therefore this hypothesis needs to be validated in future experiments.

Finally, the model predicted that STAT5B inhibits GR and that the loss of GR leads STAT5B to become a strong inhibitor of CELL-DEATH (from an ambivalent factor in the wild-type model). Lab-based results using DAS, a STAT5B inhibitor, partially validated the model predictions as, in cell lines that are relatively resistant to GC action, DEX and DAS increase cell death. This indicated that model predictions guided the research to novel findings that may have therapeutic applications. However, the *in vitro* results presented in this manuscript are limited by a lack of animal testing, primary patient cells, or clinical trials. Concurrent with this is that although chemotherapy itself often lacks consideration for the heterogeneity of the patient cohort, there has been limited opportunity in the context of the present study to explore more widely beyond the three cell lines used, although numerous *in vitro* studies have used a similar number of cell lines (34-36). Related to this is that there should be appropriate caution in attempting to extrapolate the concentrations used in the present study to doses that may see use at the clinical level. It is well-established in the literature that *in vitro* potency is not sufficient and robust enough to estimate clinically efficacious exposure (37), and that *in vitro* doses are often substantially higher (such as in the context of predicting human toxicity) (38).

In the present study DAS was used to modulate STAT5B activity and given the possibility of it affecting other pathways, future studies should support these suggestions by direct modulation of STAT5B levels and miRNA levels, although CEM leukemic cells are historically very challenging to transfect, particularly at the point of this study's origin and development (39). Despite this limitation, the results shown here shed significant light on potential routes forward for investigation and analysis of glucocorticoid sensitivity in leukemia.

In summary, miRs were incorporated into the previously established GEB052 glucocorticoid receptor computational model, resulting in the updated GAO078 model. Validation against *in silico* knockouts, DM, and STSFA analysis demonstrated high predictive accuracy. Among the model's predictions were the cytotoxic effects of DEX and DAS across various leukemia cell lines, with DAS showing therapeutic potential. Overall, these findings partially validate the model's prediction that in the absence of the GR, STAT5B becomes inhibitory towards cell death and thus CEM-C1-15 cells were more sensitive to DAS. The study has uncovered cell-type-specific treatment effects and supports the therapeutic potential of DEX/DAS combinations in GC-resistant leukemia, though caution is required in extrapolating the data to clinical settings. Future work may build on these findings by employing more complex biological models, including animal studies, to progress further towards full establishment of therapeutic value at the clinical level.

Acknowledgements

The authors are grateful to Professor Emeritus E. Brad Thompson, The University of Texas Medical Branch at Galveston, for CEM cells.

Funding

The present study was supported by the Saudi Arabia (King Saud University) and the Federal Government of Nigerian (FGN) Tertiary Education Trust Fund (TET-Fund; grant no. TETF/ASTD/UNIV/MALETE/TSAS/2019).

Availability of data and materials

The data generated in the present study are included in the figures and/or tables of this article.

Authors' contributions

AO, MN, DMC and AF planned and performed experiments, analyzed the results and prepared the draft of the manuscript. HA analyzed the results and reviewed the manuscript. AA, EYB, CD and MKD supervised the project, formulated the hypothesis, interpreted the results and prepared the manuscript. AO, EYB and MKD confirm the authenticity of all the raw data. All authors read and approved the manuscript.

Ethics approval and consent to participate

Project was approved using the University of Salford ethical approval procedures.

Patient consent for publication

Not applicable.

Competing interests

The authors declare that they have no competing interests.

References

1. Gębarowska K, Mroczek A, Kowalczyk JR and Lejman M: MicroRNA as a prognostic and diagnostic marker in T-cell acute lymphoblastic leukemia. Int J Mol Sci 22, 5317, 2021.
2. Qattan MY, Bakker EY, Rajendran R, Chen DW, Saha V, Liu J, Zeef L, Schwartz JM, Mutti L, Demonacos C and Krstic-Demonacos M: Differential regulation of cell death pathways by the microenvironment correlates with chemoresistance and survival in leukaemia. PLoS One 12: e0178606, 2017.
3. Sudsaward S, Khunchai S, Thepmalee C, Othman A, Limjindaporn T, Yenchitsomanus PT, Mutti L, Krstic-Demonacos M and Demonacos C: Endoplasmic reticulum stress, unfolded protein response and autophagy contribute to resistance to glucocorticoid treatment in human acute lymphoblastic leukaemia cells. Int J Oncol 57: 835-844, 2020.
4. Pavlovic S, Kotur N, Stankovic B, Zukic B, Gasic V and Dokmanovic L: Pharmacogenomic and pharmacotranscriptomic profiling of childhood acute lymphoblastic leukemia: Paving the way to personalized treatment. Genes (Basel) 10, 191, 2019.
5. Olczak E, Kuryłowicz A, Wicik Z, Kołodziej P, Cąkała-Jakimowicz M, Buyanovskaya O, Ślusarczyk P, Mossakowska M and Puzianowska-Kuźnicka M: Glucocorticoid receptor (NR3C1) gene polymorphisms are associated with age and blood parameters in Polish Caucasian nonagenarians and centenarians. Exp Gerontol 116: 20-24, 2019.
6. Zhu K, Zhang Y, Zhang J, Zhou F, Zhang L, Wang S, Zhu Q, Liu Q, Wang X and Zhou L: Acetylation of Hsp90 reverses dexamethasone-mediated inhibition of insulin secretion. Toxicol Lett 320: 19-27, 2020.
7. Clayton SA, Jones SW, Kurowska-Stolarska M and Clark AR: The role of microRNAs in glucocorticoid action. J Biol Chem 293: 1865-1874, 2018.
8. Shafik RE, Abd El Wahab N, Senoun SA, Ebeid E and El Taweel MA: Expression of micro-RNA 128 and Let-7b in pediatric acute lymphoblastic leukemia cases. Asian Pac J Cancer Prev 19: 2263-2267, 2018.
9. Bakker E, Tian K, Mutti L, Demonacos C, Schwartz JM and Krstic-Demonacos M: Insight into glucocorticoid receptor signalling through interactome model analysis. PLoS Comput Biol 13: e1005825, 2017.
10. Maragkakis M, Reczko M, Simossis VA, Alexiou P, Papadopoulos GL, Dalamagas T, Giannopoulos G, Goumas G, Koukis E, Kourtis K, *et al*: DIANA-microT web server: Elucidating microRNA functions through target prediction. Nucleic Acids Res 37: W273-W276, 2009.
11. Riffo-Campos ÁL, Riquelme I and Brebi-Mieville P: Tools for sequence-based miRNA target prediction: What to choose? Int J Mol Sci 17, 1987, 2016.
12. Su G, Morris JH, Demchak B and Bader GD: Biological network exploration with Cytoscape 3. Curr Protoc Bioinformatics 47: 8.13.11-24, 2014.
13. Klamt S, Saez-Rodriguez J and Gilles ED: Structural and functional analysis of cellular networks with CellNetAnalyzer. BMC Syst Biol 1: 2, 2007.
14. Isik Z, Ersahin T, Atalay V, Aykanat C and Cetin-Atalay R: A signal transduction score flow algorithm for cyclic cellular pathway analysis, which combines transcriptome and ChIP-seq data. Mol Biosyst 8: 3224-3231, 2012.
15. Montalbo K, Stasik I, Smith CGS and Bakker EY: Computational modelling and clinical validation of an Alzheimer's-related network in brain cancer: The SKM034 model. Curr Issues Mol Biol 48: 126, 2026.
16. Harmon JM and Thompson EB: Isolation and characterization of dexamethasone-resistant mutants from human lymphoid cell line CEM-C7. Mol Cell Biol 1: 512-521, 1981.
17. Norman MR and Thompson EB: Characterization of a glucocorticoid-sensitive human lymphoid cell line. Cancer Res 37: 3785-3791, 1977.
18. Cory AH, Owen TC, Barltrop JA and Cory JG: Use of an aqueous soluble tetrazolium/formazan assay for cell growth assays in culture. Cancer Commun 3: 207-212, 1991.
19. Hattori SI, Higashi-Kuwata N, Hayashi H, Allu SR, Raghavaiah J, Bulut H, Das D, Anson BJ, Lendy EK, Takamatsu Y, *et al*: A small molecule compound with an indole moiety inhibits the main protease of SARS-CoV-2 and blocks virus replication. Nat Commun 12: 668, 2021.
20. Riva L, Yuan S, Yin X, Martin-Sancho L, Matsunaga N, Pache L, Burgstaller-Muehlbacher S, De Jesus PD, Teriete P, Hull MV, *et al*: Discovery of SARS-CoV-2 antiviral drugs through large-scale compound repurposing. Nature 586: 113-119, 2020.
21. Azasi Y, Gallagher SK, Diouf A, Dabbs RA, Jin J, Mian SY, Narum DL, Long CA, Gaur D, Draper SJ, *et al*: Bliss' and Loewe's additive and synergistic effects in Plasmodium falciparum growth inhibition by AMA1-RON2L, RH5, RIPR and CyRPA antibody combinations. Sci Rep 10: 11802, 2020.
22. Rieger AM, Nelson KL, Konowalchuk JD and Barreda DR: Modified annexin V/propidium iodide apoptosis assay for accurate assessment of cell death. J Vis Exp 24: 2597, 2011.
23. Livak KJ and Schmittgen TD: Analysis of relative gene expression data using real-time quantitative PCR and the 2(-Delta Delta C(T)) method. Methods 25: 402-408, 2001.
24. Tian K, Rajendran R, Doddananjaiah M, Krstic-Demonacos M and Schwartz JM: Dynamics of DNA damage induced pathways to cancer. PLoS One 8: e72303, 2013.
25. Amelio I, Gostev M, Knight RA, Willis AE, Melino G and Antonov AV: DRUGSURV: A resource for repositioning of approved and experimental drugs in oncology based on patient survival information. Cell Death Dis 5: e1051, 2014.
26. Yeh CH, Moles R and Nicot C: Clinical significance of microRNAs in chronic and acute human leukemia. Mol Cancer 15: 37, 2016.
27. Jyotirmayee, Kumar V and Verma M: From pumps to networks: ABC transporters in leukemia resistance and microenvironmental adaptation. Med Oncol 43, 274, 2026.
28. Hussain M, Tian K, Mutti L, Krstic-Demonacos M and Schwartz JM: The expanded p53 interactome as a predictive model for cancer therapy. Genom Comput Biol 1: e20, 2015.
29. Dyczynski M, Vesterlund M, Björklund AC, Zachariadis V, Janssen J, Gallart-Ayala H, Daskalaki E, Wheelock CE, Lehtiö J, Grandér D, *et al*: Metabolic reprogramming of acute lymphoblastic leukemia cells in response to glucocorticoid treatment. Cell Death Dis 9: 846, 2018.
30. Rellick SL, Hu G, Piktel D, Martin KH, Geldenhuys WJ, Nair RR and Gibson LF: Co-culture model of B-cell acute lymphoblastic leukemia recapitulates a transcription signature of chemotherapy-refractory minimal residual disease. Sci Rep 11: 15840, 2021.
31. Hui PY, Chen YH, Qin J and Jiang XH: PON2 blockade overcomes dexamethasone resistance in acute lymphoblastic leukemia. Hematology 27: 32-42, 2022.
32. Xiong ZY, Shen YJ, Zhang SZ and Zhu HH: A review of immunotargeted therapy for Philadelphia chromosome positive acute lymphoblastic leukaemia: Making progress in chemotherapy-free regimens. Hematology 29: 2335856, 2024.
33. Park W, Wei S, Kim BS, Kim B, Bae SJ, Chae YC, Ryu D and Ha KT: Diversity and complexity of cell death: A historical review. Exp Mol Med 55: 1573-1594, 2023.
34. Gao J, Lin C, Chen S, Mo Q, Bao C, Deng H, Chen Z, Hao W, Zhang L and Wei M: MYC Addiction as a targetable vulnerability in nelarabine-resistant T-cell acute lymphoblastic leukemia. Cancer Sci 117: 1608-1622, 2026.
35. Torigoe H, Shien K, Takeda T, Yoshioka T, Namba K, Sato H, Suzawa K, Yamamoto H, Soh J, Sakaguchi M, *et al*: Therapeutic strategies for afatinib-resistant lung cancer harboring HER2 alterations. Cancer Sci 109: 1493-1502, 2018.
36. Dubois C, Dufour R, Daumar P, Aubel C, Szczepaniak C, Blavignac C, Mounetou E, Penault-Llorca F and Bamdad M: Development and cytotoxic response of two proliferative MDA-MB-231 and non-proliferative SUM1315 three-dimensional cell culture models of triple-negative basal-like breast cancer cell lines. Oncotarget 8: 95316-95331, 2017.
37. Albrecht W: Which concentrations are optimal for in vitro testing? EXCLI J 19: 1172-1173, 2020.
38. Jansson-Löfmark R, Hjorth S and Gabrielsson J: Does in vitro potency predict clinically efficacious concentrations? Clin Pharmacol Ther 108: 298-305, 2020.
39. Zhao N, Qi J, Zeng Z, Parekh P, Chang CC, Tung CH and Zu Y: Transfecting the hard-to-transfect lymphoma/leukemia cells using a simple cationic polymer nanocomplex. J Control Release 159: 104-110, 2012.

Copyright © 2026 Othman et al. This work is licensed under a Creative Commons Attribution-NonCommercial-NoDerivatives 4.0 International (CC BY-NC-ND 4.0) License.